Computational Materials Science 152 (2018) 118–124

Contents lists available at ScienceDirect

Computational Materials Science

journal homepage: www.elsevier.com/locate/commatsci

Bridging molecular dynamics and phase-field methods for grain growth prediction

Eisuke Miyoshi[a], Tomohiro Takaki[b,*], Yasushi Shibuta[c], Munekazu Ohno[d]

[a] Graduate School of Science and Technology, Kyoto Institute of Technology, Matsugasaki, Sakyo-ku, Kyoto 606-8585, Japan
[b] Faculty of Mechanical Engineering, Kyoto Institute of Technology, Matsugasaki, Sakyo-ku, Kyoto 606-8585, Japan
[c] Department of Materials Engineering, The University of Tokyo, 7-3-1 Hongo, Bunkyo-ku, Tokyo 113-8656, Japan
[d] Division of Materials Science and Engineering, Faculty of Engineering, Hokkaido University, Kita 13, Nishi 8, Kita-ku, Sapporo, Hokkaido 060-8628, Japan

ARTICLE INFO

Keywords:
Microstructural evolution
Grain growth
Phase-field method
Molecular dynamics

ABSTRACT

To achieve a highly accurate and efficient prediction of polycrystalline grain growth, we propose a method to bridge atomistic and continuum-based simulations by converting molecular dynamics-generated atomic configurations into interfacial profiles of the phase-field model. This method enables us to perform phase-field grain growth simulations in succession to molecular dynamics nucleation simulation. Using the present method, molecular dynamics and phase-field grain growth simulations from the same initial structure are carried out and directly compared. The results of each simulation exhibit a similar tendency in terms of grain morphology and grain growth kinetics, but only after an initial short duration.

1. Introduction

When a polycrystalline material is heat-treated, grain growth occurs after completion of solidification, allotropic transformation, or recrystallization [1–3]. The microstructural evolution through grain growth is of great technological importance, since it determines the final microstructure and resultant physical properties of the material. However, experimental observation of grain growth is severely limited by high temperatures and optically opaque conditions. Therefore, numerical simulations are often used to investigate the details of this phenomenon [3,4].

Grain growth simulations can be classified into two categories: atomistic simulations using molecular dynamics [5–11] or the phase-field crystal method [12–15]; and continuum-based treatments, including the phase-field [8,16–21], vertex or front-tracking [22–24], or Monte-Carlo [17,25–27] methods. Atomistic simulations can model the spontaneous nucleation process that precedes grain growth. Furthermore, thanks to recent advances in high-performance computing using graphics processing units (GPUs) and parallel computation [28–30], it is now possible to simulate the consecutive processes of nucleation, solidification, and grain growth on a sub-continuum scale using MD, as reported in our previous studies [9,11,31]. This is a major advantage of atomistic simulation, since grain growth behavior is greatly affected by the initial microstructure [32,33]. However, because grain growth is a very slow process, it is difficult to model it with atomistic methods until the late stages, owing to the limited timescales they can handle. On the other hand, continuum-based models allow for long-term observation of grain growth because of their computational efficiency. In particular, the multi-phase-field (MPF) model [34,35], which is an extension of the phase-field model to multi-phase and polycrystalline systems, has been widely employed in recent years and can accurately and efficiently simulate grain growth. Nevertheless, similar to other continuum-based models, the MPF model cannot directly reproduce the nucleation phenomenon. Given the dependence of grain growth behaviors on the initial structure, there is a pressing need for a means of providing realistic initial structures for MPF simulation. In addition, the results of MPF grain growth simulations have so far been discussed only in terms of statistics such as the average and distribution of grain sizes. However, in order to further improve the accuracy of the MPF model, it is necessary to establish a method that can test the validity of the results with respect to individual grain behaviors.

Based on this background, we aim to enable more accurate and efficient prediction of grain growth by developing a novel combined approach that exploits the merits of atomistic and continuum simulations. In this approach, nucleation is simulated by the MD method, and the obtained microstructure is then used as the initial structure for MPF grain growth simulation. This direct bridging is achieved by a sub-continuum-scale atomistic simulation based on high-performance computing techniques, and appears to be a promising approach in light of the recent rapid progress in computer performance. As a first step

* Corresponding author.
E-mail address: takaki@kit.ac.jp (T. Takaki).

https://doi.org/10.1016/j.commatsci.2018.05.046
Received 26 March 2018; Received in revised form 22 May 2018; Accepted 22 May 2018
Available online 31 May 2018

toward this goal, focusing on two-dimensional problems, this study proposes a method to convert MD-generated atomic configurations into phase-field profiles of the MPF model. Furthermore, MPF and MD grain growth simulations are directly compared using the proposed method, and the similarities and differences of each simulation result are discussed.

2. Methodology

The MPF model and large-scale MD simulation data used in this study are briefly described, after which we present a method for creating MPF interfacial profiles from the MD data.

2.1. Multi-phase-field model

The generalized MPF model proposed by Steinbach and Pezzolla [35] is employed for phase-field grain growth simulations. This model represents a polycrystalline system including N grains through N phase-field variables ϕ_i ($i = 1, 2,\ldots, N$), which take a value of 1 in the ith grain and 0 in the other grains, with smooth changing from 1 to 0 at the grain boundaries. The migration of grain boundaries is reproduced by calculating the time evolution of ϕ_i at each spatial point under the constraint of free energy minimization. When considering grain growth processes driven only by the grain boundary curvatures, the time-evolution equation is given as:

$$\frac{\partial \phi_i}{\partial t} = -\frac{2}{n}\sum_{j=1}^{n} M_{ij}^{\phi} \sum_{k=1}^{n} \left\{ (W_{ik} - W_{jk})\phi_k + \frac{1}{2}(a_{ik}^2 - a_{jk}^2)\nabla^2\phi_k \right\}, \quad (1)$$

where n is the number of nonzero phase-field variables at the specified point, and M_{ij}^{ϕ}, W_{ij}, and a_{ij} denote the phase-field mobility, barrier height, and gradient coefficient of the boundary between the ith and jth grains, respectively. These parameters are related to the thickness (δ), energy (σ_{ij}), and mobility (M_{ij}) of the i-j grain boundary through the following equations: $M_{ij}^{\phi} = \pi^2 M_{ij}/(8\delta)$, $W_{ij} = 4\sigma_{ij}/\delta$, and $a_{ij} = 2(2\delta\sigma_{ij})^{1/2}/\pi$. Note that the computation of the original MPF model is likely to become unstable in the cases where grain boundary energy and/or mobility are not uniform. Therefore, under such conditions, we employ the higher-order modifications proposed in a previous study [36] to prevent the MPF computation from being unstable.

2.2. Molecular dynamics simulation data

As the MD data, we use the results of a previous quasi-two-dimensional MD simulation [9] on the solidification of pure iron. In this simulation, an undercooled iron melt consisting of 1,037,880 atoms was held at 1400 K in a thin periodic boundary cell ($53.4 \times 53.4 \times 4.3\,\mathrm{nm}^3$), and computations of up to 10,000 ps were performed on the GPU supercomputer TSUBAME2.5 at the Tokyo Institute of Technology. The interatomic interaction between iron atoms was represented using the Finnis-Sinclair potential [37], which is one of the best-established potentials for body-centered-cubic (bcc) metals. For reference, some snapshots of solidification and early-stage grain growth in the MD simulation are provided in Fig. 1, where atoms with the bcc configuration are colored blue, other atoms being shown in white. More details of the simulation methodology and results can be found in Ref. [9]. In the present study, the geometric information of grains is extracted as follows, in line with our previous study [11]. First, atoms with bcc configuration are identified by the common neighbor analysis [38,39]. Next, the principal axes (directions to the second-nearest-neighbor atoms) of each bcc atom are described as three Euler angles (α, β, γ) with respect to the global coordinate axes. Then, the disorientation angles between two neighboring bcc atoms are determined by a rotation operation [40] that makes their principal axes coincide. The bcc atoms within a disorientation angle of less than 2° are classified as belonging to the same grain.

2.3. Procedures to convert atomic configuration into phase-field profiles

To perform MPF grain growth simulations after the MD solidification simulation, the geometric information obtained from the MD analysis is reduced to two-dimensional phase-field profiles by the following procedures.

(i) Discretization by difference grids. A cross section ($53.4 \times 53.4\,\mathrm{nm}^2$) of the MD computation cell is divided into two-dimensional difference grids. Grains are assigned to each grid point as follows. First, an area within the radius R from a grid point of interest is searched throughout the thickness (4.3 nm) of the MD cell, and bcc atoms present in the search area are extracted. The next step is to determine to which grain the extracted atoms belong. Then, a grain that occupies the most atoms is assigned to the grid point of interest. In the discretized polycrystalline system, the crystal coordinate axes of a given grain are determined by the average Euler angles of all the bcc atoms constituting the grain; the determined coordinate axes are used to calculate disorientation angles in the MPF simulation.

(ii) Relaxation simulation. In the two-dimensional polycrystalline system obtained in step (i), there exists no interfacial thickness, and the phase-field variables change discontinuously at the grain boundaries. Therefore, MPF relaxation simulation without the curvature effect is performed, through which diffuse interfaces with equilibrium profiles in the interfacial normal directions are created while maintaining the grain configurations. The curvature effect is removed by subtracting the curvature contribution $\nabla\phi_k|\nabla\cdot(\nabla\phi_k/|\nabla\phi_k|)$ from the Laplacian term $\nabla^2\phi_k$ in Eq. (1) (for more detail, see Appendix A).

3. Results and discussion

We create MPF interfacial profiles from the MD data using the above-described method, and test the validity of the method. Then, grain growth simulations by the MD and MPF methods are directly compared. For this purpose, we use a MD-generated solidified microstructure (at time $t = 1000$ ps) shown in Fig. 2 (a). In this microstructure, grains generally exhibit columnar shapes in the thickness direction. Here, bcc atoms are colored in accordance with the disorientation angle relative to the global coordinate axes, Θ, whereas other atoms are shown in black. In the MPF simulations, the computational domain is divided into 512×512 square regular grids with a size of $\Delta x = 0.1043$ nm. The grain boundary thickness, δ, is set to $6\Delta x = 0.626$ nm, and the time increment, Δt, is set to 0.1 ps. For the grain boundary energy, σ, and mobility, M, both isotropic (uniform) and anisotropic (disorientation-dependent) conditions are employed. Okita and Shibuta [10] estimated the product of boundary properties, $\sigma \times M$, to be $6.48 \times 10^{-9}\,\mathrm{m^2\,s^{-1}}$ on average by fitting the von Neumann-Mullins relation [41,42] to their MD data, which is used in this study. In the present simulation, assuming a typical σ value of $1\,\mathrm{J\,m^{-2}}$ for pure iron [43], we use $\sigma = 1\,\mathrm{J\,m^{-2}}$ and $M = 6.48 \times 10^{-9}\,\mathrm{m^4\,J^{-1}\,s^{-1}}$ for isotropic grain growth. In the case of anisotropic growth, σ and M are expressed as functions of the disorientation angle between neighboring grains, θ:

$$\sigma(\theta) = \begin{cases} \sigma_{\mathrm{H}} \frac{\theta}{20}\left\{1 - \ln\left(\frac{\theta}{20}\right)\right\} & (\theta \leqslant 20^\circ), \\ \frac{2}{3}\sigma_{\mathrm{H}} & (57^\circ \leqslant \theta \leqslant 63^\circ), \\ \sigma_{\mathrm{H}} & (\text{otherwise}), \end{cases} \quad (2)$$

$$M(\theta) = \begin{cases} M_{\mathrm{H}}\left[1 - \exp\left\{-5\left(\frac{\theta}{20}\right)^4\right\}\right] & (\theta \leqslant 20^\circ), \\ 1.5M_{\mathrm{H}} & (57^\circ \leqslant \theta \leqslant 63^\circ), \\ M_{\mathrm{H}} & (\text{otherwise}), \end{cases} \quad (3)$$

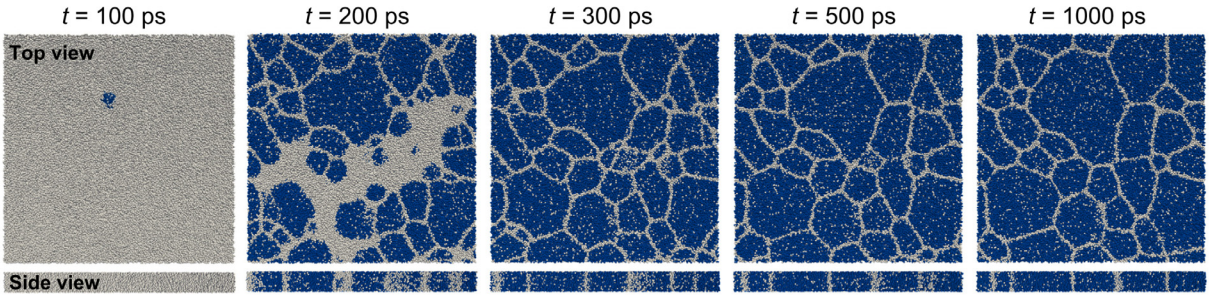

Fig. 1. Snapshots of the atomic configuration during nucleation, solidification, and early-stage grain growth from undercooled iron melt, as obtained by a quasi-two-dimensional MD simulation [9]. Atoms with the bcc configuration are colored blue, whereas other atoms are shown in white. (For interpretation of the references to colour in this figure legend, the reader is referred to the web version of this article.)

where σ_H and M_H denote the energy and mobility, respectively, of general high-angle grain boundaries. Here, low-angle ($\theta \leq 20^\circ$) boundary energy and mobility are modeled using the Read-Shockley relation [44] and the sigmoidal relation reported by Humphreys [45]. Special boundaries with Σ3 misorientations, which tend to exhibit relatively low energy and high mobility, are considered in the vicinity of $\theta = 60^\circ$ [46–48]; the energy and mobility of the special boundaries are assumed to be $2/3\sigma_H$ and $1.5M_H$, respectively. The σ_H value is set to a typical $1\,J\,m^{-2}$, similar to the isotropic simulation. On the other hand, M_H is treated as an adjustment parameter and set to $6.67\,m^4\,J^{-1}\,s^{-1}$, such that the average of the product $\sigma \times M$ is almost same as in the isotropic case ($6.48 \times 10^{-9}\,m^2\,s^{-1}$, see above).

3.1. Creation of initial phase-field profiles

Fig. 2(b) and (c) show the phase-field polycrystalline structures before and after the relaxation simulation, respectively, as created from the MD-generated microstructure shown in Fig. 2(a). Here, grains are colored in accordance with disorientation angle Θ, whereas diffuse interfaces are visualized by the sum of the squared phase fields, $\Sigma_{\phi i}{}^2$. The search area radius, R, in procedure (i) (see Section 2.3) was set to $10\Delta x$, and the relaxation simulation in procedure (ii) was performed using isotropic grain boundary properties until the phase-field profiles were unchanged. In Fig. 2(c), a slight deviation from the MD data can be observed for the grain boundary indicated by the yellow frame; this is attributable to the not-fully columnar shapes of grains constituting this boundary in the MD cell. However, overall, the atomic configuration is converted well into phase-field profiles. To further confirm the validity of the results, we plotted (Fig. 3(a)) an example of the variations of one-dimensional phase-field profiles before and after the relaxation simulation. Here, for grain 1 (indicated by the red frame in Fig. 2(c)), the values of the corresponding phase field (ϕ_1) are plotted along a line $y = 20\Delta x$, on which the interface of the grain is perpendicular to the x-axis. As shown in Fig. 3(a), the distribution of the ϕ_1 value after relaxation was in good agreement with the theoretical one-dimensional equilibrium profile, $\phi_{eq} = \frac{1}{2}[1-\sin\{\pi(x-x_c)/\delta\}]$ (x_c: x-coordinate of the center of the interface), which is depicted by a black dashed line in the figure. Next, we calculated the temporal variations in the areas (A_i (t)) of each grain during the relaxation simulation; the maximum relative error, ε_{max}, of grain areas with respect to their initial values (i.e., $\varepsilon_{max} = \max\{|(A_i(t)-A_i(0))/A_i(0)||i = 1, 2, \ldots\}$) is given in Fig. 3(b) as a function of time. The changes in grain area during the relaxation were at most around 0.1%, exhibiting a high area conservation.

3.2. Grain growth in molecular dynamics and phase-field simulations

The results summarized above conclude that our present method allows for the creation of MPF interfacial profiles from atomic information while maintaining the microstructural morphology. This conversion enables a direct bridging between the MD and MPF methods in a sequential simulation from nucleation and solidification to grain growth. In addition, this conversion allows direct comparison of the MD and MPF simulations of grain growth, from which one may check the validity of the MPF method and gain insight into aspects of grain growth that are not well modeled by current MPF simulations. Hence, we performed MD and MPF grain growth simulations until time

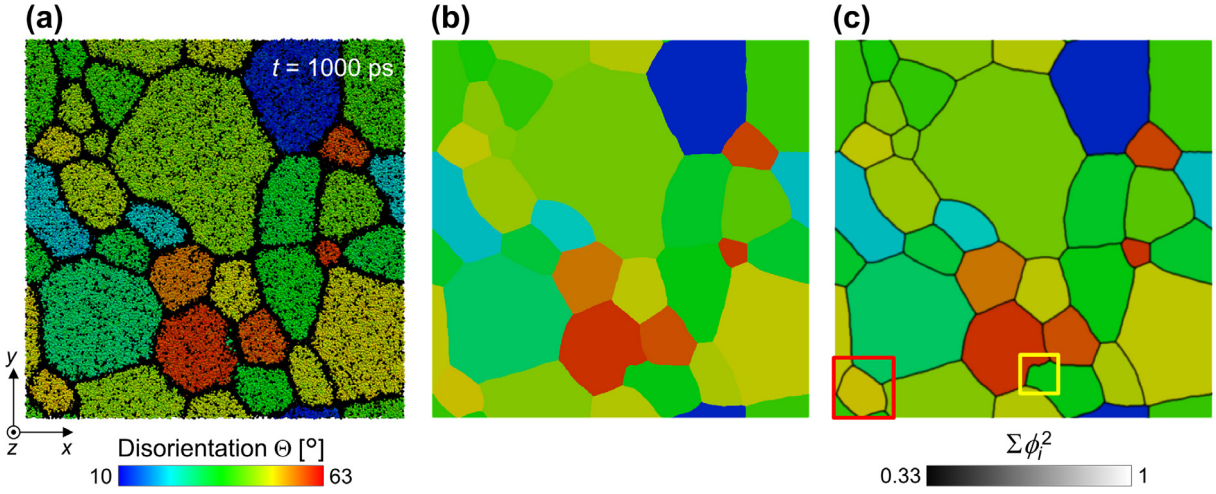

Fig. 2. Creation of an initial structure for MPF grain growth simulations from MD data. (a) MD-generated solidified microstructure at time $t = 1000$ ps. (b) Polycrystalline system created by discretizing the atomic configuration shown in (a) into two-dimensional difference grid points. (c) MPF interfacial profiles obtained through the relaxation simulation starting from (b). Red and yellow frames in (c) indicate a grain and a grain boundary specifically mentioned in the main text. (For interpretation of the references to colour in this figure legend, the reader is referred to the web version of this article.)

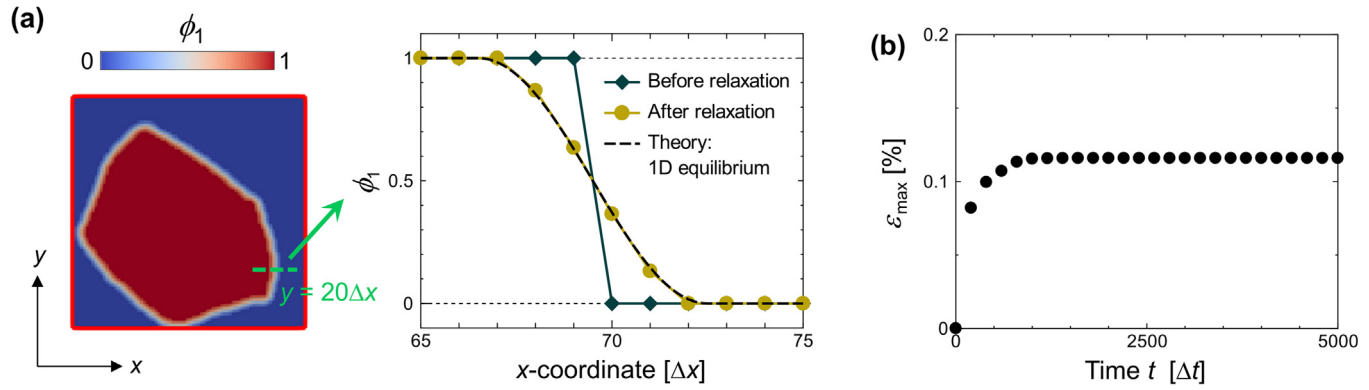

Fig. 3. Validation of the proposed method to create an initial structure for MPF simulations. (a) Phase-field profiles of grain 1 (indicated by a red frame in Fig. 2 (c)) before and after relaxation. (b) Temporal variation of ε_{max} during the relaxation simulation. (For interpretation of the references to colour in this figure legend, the reader is referred to the web version of this article.)

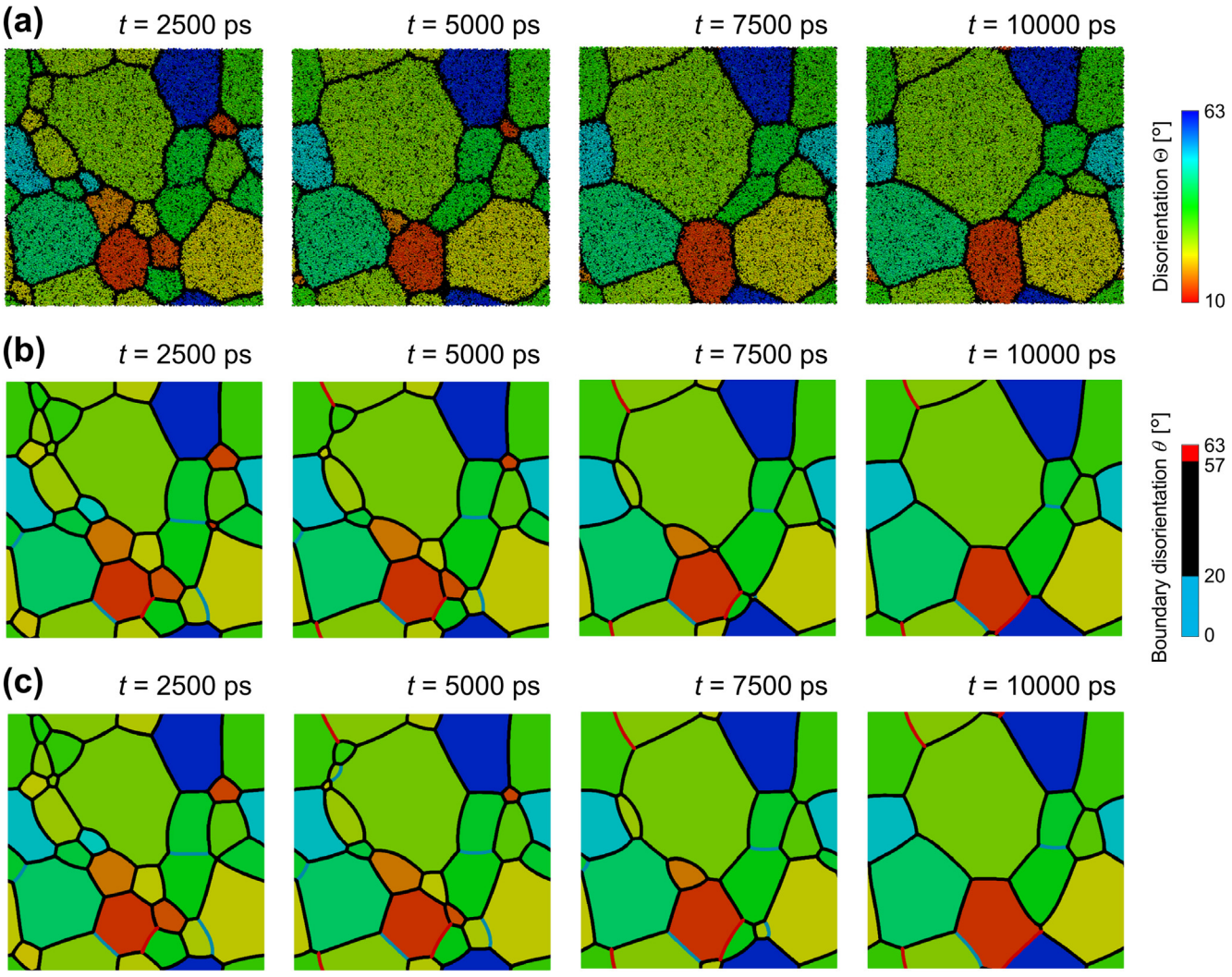

Fig. 4. Evolved microstructures in the grain growth simulations using the (a) MD method and (b, c) MPF method with (b) isotropic and (c) anisotropic grain boundary properties. The initial structures for the MD and MPF simulations are those shown in Fig. 2 (a) and (c), respectively.

t = 10,000 ps, starting from the solidified microstructures (at t = 1000 ps) shown in Fig. 2(a) and (c). Fig. 4 displays some snapshots of the microstructural evolutions in (a) the MD simulation and (b, c) the MPF simulations, with (b) isotropic and (c) anisotropic grain boundary properties. The temporal variations in the number of remaining grains during these simulations are shown in Fig. 5; some increases in grain number observed for the MD simulation can be ascribed to the thermal fluctuation of atoms, which sometimes cause miscounting of low-angle grain boundaries. In Fig. 4(b) and (c), grain boundaries are colored in accordance with the boundary disorientation angle θ (blue: low-angle boundaries of $\theta \leq 20^\circ$; red: Σ3 boundaries of $57^\circ \leq \theta \leq 63^\circ$; black: general high-angle boundaries). More detailed data for the evolution

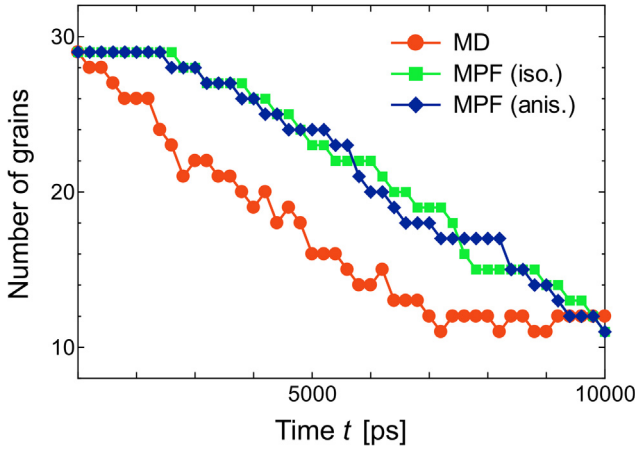

Fig. 5. Temporal variations of the number of remaining grains during the grain growth simulations shown in Fig. 4. Some increases in grain number observed for the MD result are ascribed to the thermal fluctuation of atoms, which can cause miscount of low-angle grain boundaries.

processes are provided as a Video In The Supplementary Material.

At relatively late stages of grain growth, the present MD and MPF simulation results show a similar tendency. For instance, as confirmed in the panels on the right side of Fig. 4, the microstructures at the late stage (t = 10,000 ps) obtained from the MD and MPF simulations are in moderately good agreement with each other, in that almost the same grains remain, and their topologies (number of edges per grain) and sizes are similar. The effect of the introduction of anisotropic grain boundary properties was small; this is probably attributable to the small fraction of low-angle and Σ3 boundaries in the MD-generated initial structure, in addition to the limited possibility of forming new low-angle or Σ3 boundaries due to the small number of initial grains. If the initial fractions of such boundaries or the initial grain number increases, the effect of the anisotropic properties would become stronger as reported from larger-scale MPF simulations in the previous studies [49–51]. Additionally, as shown in Fig. 5, except for an initial short duration, the slopes of the grain number versus time curves for the MPF simulations corresponded well to that for the MD simulation. This suggests that the MPF grain growth reached almost the same kinetics as the MD growth. By contrast, in the early stages of grain growth, the shrinkage of relatively small grains proceeded more slowly in the MPF simulations than in the MD simulation (Fig. 4). Consequently, the decrease rate in grain number during the early stages was visibly lower for the MPF simulations (Fig. 5). This initial delay in MPF simulation was also observed when the initial structure was created from MD-generated structures at times other than 1000 ps. For example, Fig. 6(b) plots the grain number versus time in additional MPF simulations, which started from the phase-field structures in Fig. 6(a) corresponding to the MD data for t = 2000 ps and 3000 ps. Again, one can see that the MPF simulations initially show lower decrease rate in grain number compared to the MD. The cause of the delay may be attributable to the simplification of grain boundary anisotropy in the MPF simulations. The simple anisotropy models (Eqs. (2) and (3)) employed in the present study assume that the properties of general high-angle grain boundaries are isotropic. However, in reality, grain boundary properties vary considerably, even in the case of high-angle boundaries, depending on the five parameters that describe boundary structures [52]. Indeed, although most of the grain boundaries present in our MD simulation are general high-angle boundaries, many boundaries do not intersect at 120° at their triple junctions (as required for local equilibrium under the condition of uniform boundary properties). Thus, when MPF simulation with the simple anisotropy models starts from the MD-generated structure, grain growth may be delayed owing to the transient time required to fulfill the local equilibrium of grain

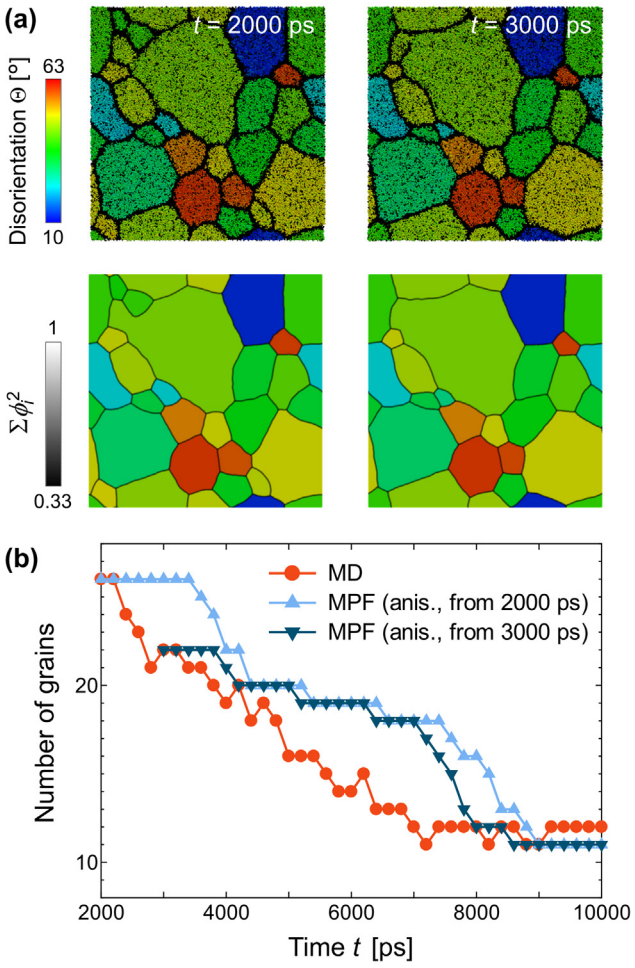

Fig. 6. (a) Re-creation of initial structures for MPF grain growth simulations from MD data. Top: MD-generated solidified microstructures at times t = 2000 and 3000 ps. Bottom: MPF profiles as created from the MD data corresponding to the upper row. (b) Temporal variations of the number of remaining grains during the MD and MPF grain growth simulations. The MPF simulations start from the initial structures shown in (a) using anisotropic grain boundary properties.

boundaries. In order to avoid this initial short delay, a detailed database of the structure–property relationships of grain boundaries would need to be constructed and integrated into the MPF model. Nevertheless, the long-term behavior of grain growth can be said to be well expressed by the current MPF simulation.

Finally, we want to briefly note additional grain growth-related factors that were not addressed here. This study focused only on curvature-driven grain growth in the MPF model since there were no significant changes in the grain disorientations during the current MD simulation (see Video in the Supplementary Material). In some cases, however, grain rotation has a significant effect on growth processes and could be required to be considered in continuum models. One of the possible ways to account for grain rotation in phase-field simulation is the usage of so-called orientation-field models, including the Kobayashi-Warren-Carter (KWC) [53–56] and Henry-Mellenthin-Plapp (HMP) [20,57] models, which can express both the rotation and growth of grains using only two order parameters. Nevertheless, using these models, it is difficult to simulate grain growth quantitatively because the coefficients of the time-evolution equations cannot be directly related to material parameters [58], unlike the case of the MPF model. In addition, the time-evolution equations of the KWC model are singular diffusion equations and, thus, the time increment for the numerical simulations must be set very small. Another possible way is to couple a

phase-field equation and an additional evolution equation for crystal orientation, as recently proposed by Vuppuluri [59]. Such coupling is also reported to be useful for introducing other important atomic-level phenomena, such as the generation and density evolution of defects, into phase-field simulation [60]. The adaptation of the MPF model to the coupling will be addressed elsewhere.

4. Conclusions

In summary, the method proposed here successfully converted a MD-generated atomic configuration into MPF profiles, enabling the direct bridging of MD and phase-field methods for grain growth simulations; this was achieved by utilizing sub-continuum-scale MD simulation results obtained with high-performance computing. Our new approach has important implications for multi-scale modeling. That is, the space scale of the MD method already reaches that of the phase-field method in our approach, whereas in conventional multi-scale modeling, only averaged values of physical properties from the smaller-scale method are extracted as representative parameters and transferred to the larger-scale method. The direct mapping of the information from atomistic to continuum simulations proposed in this study expands the potential use of multi-scale modeling in the future. Moreover, ongoing improvement of numerical modeling will further enhance the usefulness of our proposed method in materials design. For example, we plan to investigate the structure-property relationships of grain boundaries via MD bicrystal simulations [8,49] and construct a database for MPF simulation, since we found some discrepancies between the MD and MPF results in early-stage grain growth that are probably due to the complexity of anisotropic grain boundary properties. The present method will also be useful to accurately transfer MD-determined grain boundary properties to the MPF model by directly comparing MD and MPF simulations.

Acknowledgements

This research was supported by Grant-in-Aids for Scientific Research (B) (No. 16H04490) and (A) (No. 17H01237) and for JSPS Fellows (No. 17J06356) from the Japan Society for the Promotion of Science (JSPS), the Joint Usage/Research Center for Interdisciplinary Large-scale Information Infrastructures, and the High Performance Computing Infrastructure in Japan (Project ID: jh170018-NAH), and MEXT as a social and scientific priority issue (Creation of new functional devices and high-performance materials to support next-generation industries) to be tackled using the post-K computer.

Appendix A. A. Removal of curvature effect from the multi-phase-field model

We describe in detail how to remove the curvature effect from the MPF model. In the MPF equation (Eq. (1)), the contribution of the interfacial curvature κ_i (i: grain number) is included in the Laplacian term, $\nabla^2\phi_i$. Considering the unit normal vector $\mathbf{n}_i = \nabla\phi_i/|\nabla\phi_i|$ of the interface of the ith grain, κ_i can be expressed as [61]:

$$\kappa_i = \nabla\cdot\mathbf{n}_i = \nabla\cdot\left(\frac{\nabla\phi_i}{|\nabla\phi_i|}\right) = \frac{1}{|\nabla\phi_i|}\left(\nabla^2\phi_i - \frac{\nabla\phi_i\cdot\nabla|\nabla\phi_i|}{|\nabla\phi_i|}\right). \tag{A.1}$$

Hence, $\nabla^2\phi_i$ can be written as the sum of two terms with and without κ_i:

$$\nabla^2\phi_i = |\nabla\phi_i|\kappa_i + \frac{\nabla\phi_i\cdot\nabla|\nabla\phi_i|}{|\nabla\phi_i|} = |\nabla\phi_i|\nabla\cdot\left(\frac{\nabla\phi_i}{|\nabla\phi_i|}\right) + \frac{\nabla\phi_i\cdot\nabla|\nabla\phi_i|}{|\nabla\phi_i|}. \tag{A.2}$$

The first term on the right-hand side of Eq. (A.2) represents the curvature contribution. By subtracting this from the Laplacian term in Eq. (1), we obtain a reduced form of the MPF equation that does not include the curvature effect:

$$\frac{\partial\phi_i}{\partial t} = -\frac{2}{n}\sum_{j=1}^{n} M_{ij}^{\phi}\sum_{k=1}^{n}\left\{(W_{ik}-W_{jk})\phi_k + \frac{1}{2}(a_{ik}^2-a_{jk}^2)\left(\nabla^2\phi_k - |\nabla\phi_k|\nabla\cdot\left(\frac{\nabla\phi_k}{|\nabla\phi_k|}\right)\right)\right\}. \tag{A.3}$$

Appendix B. Supplementary material

Supplementary data associated with this article can be found, in the online version, at http://dx.doi.org/10.1016/j.commatsci.2018.05.046.

References

[1] F.J. Humphreys, M. Hatherly, Recrystallisation and Related Annealing Phenomena, second ed., Elsevier Ltd., Oxford, 2004.
[2] H.V. Atkinson, Overview no. 65. Theories of normal grain growth in pure single phase systems, Acta Metall. 36 (1988) 469–491.
[3] M.A. Miodownik, A review of microstructural computer models used to simulate grain growth and recrystallisation in aluminium alloys, J. Light Met. 2 (2002) 125–135.
[4] D. Raabe, Computational Materials Science, Wiley-VCH, Weinheim, 1998.
[5] A.J. Haslam, S.R. Phillpot, D. Wolf, D. Moldovan, H. Gleiter, Mechanisms of grain growth in nanocrystalline fcc metals by molecular-dynamics simulation, Mater. Sci. Eng. A 318 (2001) 293–312.
[6] D. Farkas, S. Mohanty, J. Monk, Linear grain growth kinetics and rotation in nanocrystalline Ni, Phys. Rev. Lett. 98 (2007) 4–7.
[7] E.A. Holm, S.M. Foiles, How grain growth stops : a mechanism for grain-growth stagnation in pure materials, Science 328 (2010) 1138–1141.
[8] M.R. Tonks, Y. Zhang, S.B. Biner, P.C. Millett, X. Bai, Guidance to design grain boundary mobility experiments with molecular dynamics and phase-field modeling, Acta Mater. 61 (2013) 1373–1382.
[9] Y. Shibuta, K. Oguchi, T. Takaki, M. Ohno, Homogeneous nucleation and microstructure evolution in million-atom molecular dynamics simulation, Sci. Rep. 5 (2015) 13534.
[10] S. Okita, Y. Shibuta, Grain growth in large-scale molecular dynamics simulation: linkage between atomic configuration and von Neumann-Mullins relation, ISIJ Int. 56 (2016) 2199–2207.
[11] Y. Shibuta, S. Sakane, E. Miyoshi, S. Okita, T. Takaki, M. Ohno, Heterogeneity in homogeneous nucleation from billion-atom molecular dynamics simulation of solidification of pure metal, Nat. Commun. 8 (2017) 10.
[12] T. Hirouchi, T. Takaki, Y. Tomita, Development of numerical scheme for phase field crystal deformation simulation, Comput. Mater. Sci. 44 (2009) 1192–1197.
[13] K.A. Wu, P.W. Voorhees, Phase field crystal simulations of nanocrystalline grain growth in two dimensions, Acta Mater. 60 (2012) 407–419.
[14] M. Bjerre, J.M. Tarp, L. Angheluta, J. Mathiesen, Rotation-induced grain growth and stagnation in phase-field crystal models, Phys. Rev. E 88 (2013) 020401.
[15] A. Yamanaka, K. McReynolds, P.W. Voorhees, Phase field crystal simulation of grain boundary motion, grain rotation and dislocation reactions in a BCC bicrystal, Acta Mater. 133 (2017) 160–171.
[16] D. Fan, L.-Q. Chen, Computer simulation of grain growth using a continuum field model, Acta Mater. 45 (1997) 611–622.
[17] Y. Suwa, Y. Saito, Computer simulation of grain growth in three dimensions by the phase field model and the Monte Carlo method, Mater. Trans. 46 (2005) 1214–1220.
[18] S.G. Kim, D.I. Kim, W.T. Kim, Y.B. Park, Computer simulations of two-dimensional and three-dimensional ideal grain growth, Phys. Rev. E 74 (2006) 061605.
[19] Y. Suwa, Y. Saito, H. Onodera, Parallel computer simulation of three-dimensional grain growth using the multi-phase-field model, Mater. Trans. 49 (2008) 704–709.

[20] B. Korbuly, T. Pusztai, H. Henry, M. Plapp, M. Apel, L. Gránásy, Grain coarsening in two-dimensional phase-field models with an orientation field, Phys. Rev. E 95 (2017) 053303.
[21] E. Miyoshi, T. Takaki, M. Ohno, Y. Shibuta, S. Sakane, T. Shimokawabe, T. Aoki, Ultra-large-scale phase-field simulation study of ideal grain growth, npj Comput, Mater. 3 (2017) 25.
[22] K. Fuchizaki, T. Kusaba, K. Kawasaki, Computer modelling of three-dimensional cellular pattern growth, Philos. Mag. B 71 (1995) 333–357.
[23] D. Weygand, Y. Bréchet, J. Lépinoux, W. Gust, Three-dimensional grain growth: a vertex dynamics simulation, Philos. Mag. B 79 (1999) 703–716.
[24] J.K. Mason, E.A. Lazar, R.D. MacPherson, D.J. Srolovitz, Geometric and topological properties of the canonical grain growth microstructure, Phys. Rev. E 92 (2015) 063308.
[25] M.P. Anderson, D.J. Srolovitz, G.S. Grest, P.S. Sahni, Computer simulation of grain growth—I. Kinetics, Acta Metall. 32 (1984) 783–791.
[26] D.J. Srolovitz, M.P. Anderson, P.S. Sahni, G.S. Grest, Computer simulation of grain growth—II. Grain size distribution, topology, and local dynamics, Acta Metall. 32 (1984) 793–802.
[27] D. Zöllner, P. Streitenberger, Three-dimensional normal grain growth: Monte Carlo Potts model simulation and analytical mean field theory, Scr. Mater. 54 (2006) 1697–1702.
[28] T. Shimokawabe, T. Takaki, T. Endo, A. Yamanaka, N. Maruyama, T. Aoki, A. Nukada, S. Matsuoka, Peta-scale phase-field simulation for dendritic solidification on the TSUBAME 2.0 supercomputer, in: Proceedings of 2011 International Conference for High Performance Computing, Networking, Storage and Analysis, ACM, Seattle, 2011, pp. 1–11.
[29] T. Takaki, T. Shimokawabe, M. Ohno, A. Yamanaka, T. Aoki, Unexpected selection of growing dendrites by very-large-scale phase-field simulation, J. Cryst. Growth 382 (2013) 21–25.
[30] Y. Shibuta, M. Ohno, T. Takaki, Solidification in a supercomputer: from crystal nuclei to dendrite assemblages, JOM 67 (2015) 1793–1804.
[31] Y. Shibuta, S. Sakane, T. Takaki, M. Ohno, Submicrometer-scale molecular dynamics simulation of nucleation and solidification from undercooled melt: linkage between empirical interpretation and atomistic nature, Acta Mater. 105 (2016) 328–337.
[32] A.D. Rollett, D.J. Srolovitz, M.P. Anderson, Simulation and theory of abnormal grain growth— anisotropic grain boundary energies and mobilities, Acta Metall. 37 (1989) 1227–1240.
[33] Y. Suwa, Y. Saito, H. Onodera, Three-dimensional phase field simulation of the effect of anisotropy in grain-boundary mobility on growth kinetics and morphology of grain structure, Comput. Mater. Sci. 40 (2007) 40–50.
[34] I. Steinbach, F. Pezzolla, B. Nestler, M. Seeßelberg, R. Prieler, G.J. Schmitz, J.L.L. Rezende, A phase field concept for multiphase systems, Physica D 94 (1996) 135–147.
[35] I. Steinbach, F. Pezzolla, A generalized field method for multiphase transformations using interface fields, Physica D 134 (1999) 385–393.
[36] E. Miyoshi, T. Takaki, Validation of a novel higher-order multi-phase-field model for grain-growth simulations using anisotropic grain-boundary properties, Comput. Mater. Sci. 112 (2016) 44–51.
[37] M.W. Finnis, J.E. Sinclair, A simple empirical *N*-body potential for transition metals, Philos. Mag. A 50 (1984) 45–55.
[38] Y. Shibuta, T. Suzuki, A molecular dynamics study of the phase transition in bcc metal nanoparticles, J. Chem. Phys. 129 (2008) 144102.
[39] A. Stukowski, Structure identification methods for atomistic simulations of crystalline materials, Model. Simul. Mater. Sci. Eng. 20 (2012) 045021.
[40] J.K. Mason, C.A. Schuh, The generalized Mackenzie distribution: disorientation angle distributions for arbitrary textures, Acta Mater. 57 (2009) 4186–4197.
[41] J. von Neumann, Discussion—shape of metal grains, in: C. Herring (Ed.), Metal Interfaces, American Society for Metals, Cleveland, 1952, pp. 108–110.
[42] W.W. Mullins, Two-dimensional motion of idealized grain boundaries, J. Appl. Phys. 27 (1956) 900–904.
[43] Y. Shibuta, S. Takamoto, T. Suzuki, A molecular dynamics study of the energy and structure of the symmetric tilt boundary of iron, ISIJ Int. 48 (2008) 1582–1591.
[44] W.T. Read, W. Shockley, Dislocation models of crystal boundaries, Phys. Rev. 78 (1950) 275–289.
[45] F.J. Humphreys, A unified theory of recovery, recrystallization and grain growth, based on the stability and growth of cellular microstructures—I. The basic model, Acta Mater. 45 (1997) 4231–4240.
[46] D.L. Olmsted, S.M. Foiles, E.A. Holm, Survey of computed grain boundary properties in face-centered cubic metals: I. Grain boundary energy, Acta Mater. 57 (2009) 3694–3703.
[47] D.L. Olmsted, E.A. Holm, S.M. Foiles, Survey of computed grain boundary properties in face-centered cubic metals—II: Grain boundary mobility, Acta Mater. 57 (2009) 3704–3713.
[48] S. Ratanaphan, D.L. Olmsted, V.V. Bulatov, E.A. Holm, A.D. Rollett, G.S. Rohrer, Grain boundary energies in body-centered cubic metals, Acta Mater. 88 (2015) 346–354.
[49] M. Upmanyu, G.N. Hassold, A. Kazaryan, E.A. Holm, Y. Wang, B. Patton, D.J. Srolovitz, Boundary mobility and energy anisotropy effects on microstructural evolution during grain growth, Interface Sci. 10 (2002) 201–216.
[50] Y. Suwa, Y. Saito, Phase field simulation of the effect of anisotropy in grain boundary energy on growth kinetics and morphology of grain structure, Mater. Trans. 46 (2005) 1208–1213.
[51] E. Miyoshi, T. Takaki, Multi-phase-field study of the effects of anisotropic grain-boundary properties on polycrystalline grain growth, J. Cryst. Growth 474 (2017) 160–165.
[52] D.M. Saylor, A. Morawiec, G.S. Rohrer, Distribution of grain boundaries in magnesia as a function of five macroscopic parameters, Acta Mater. 51 (2003) 3663–3674.
[53] R. Kobayashi, J.A. Warren, W.C. Carter, Vector-valued phase field model for crystallization and grain boundary formation, Physica D 119 (1998) 415–423.
[54] J.A. Warren, W.C. Carter, R. Kobayashi, A phase field model of the impingement of solidifying particles, Physica A 261 (1998) 159–166.
[55] R. Kobayashi, J.A. Warren, W.C. Carter, A continuum model of grain boundaries, Physica D 140 (2000) 141–150.
[56] J.A. Warren, R. Kobayashi, A.E. Lobkovsky, W.C. Carter, Extending phase field models of solidification to polycrystalline materials, Acta Mater. 51 (2003) 6035–6058.
[57] H. Henry, J. Mellenthin, M. Plapp, Orientation-field model for polycrystalline solidification with a singular coupling between order and orientation, Phys. Rev. B 86 (2012) 054117.
[58] A. Ask, S. Forest, B. Appolaire, K. Ammar, O.U. Salman, A Cosserat crystal plasticity and phase field theory for grain boundary migration, J. Mech. Phys. Solids 115 (2018) 167–194.
[59] A. Vuppuluri, Theory and simulation of microstructure evolution due to simultaneous grain boundary migration and grain rotation with misorientation dependent energy and mobility, Mater. Sci. Eng. A 713 (2018) 118–124.
[60] Y. Li, S. Hu, X. Sun, M. Stan, A review: applications of the phase field method in predicting microstructure and property evolution of irradiated nuclear materials, npj Comput. Mater. 3 (2017) 16.
[61] Y. Sun, C. Beckermann, Sharp interface tracking using the phase-field equation, J. Comput. Phys. 220 (2007) 626–653.